mass spectrometry (*43*). Our study has also confirmed the absolute stereochemistry of ciguatoxins (*6*).

A preliminary toxicity study of the natural product and the synthetic compounds was carried out in mice. As expected, synthetic CTX3C (**2**) displayed LD_{50} values (~1.5 μg/kg) comparable to that of the natural form (1.3 μg/kg) (*7*). However, it is surprising that the protected intermediate **28** did not exhibit detectable toxicity, which suggests that our synthetic route is fortunately nontoxic until the final deprotection step.

The total synthesis of CTX3C was achieved via the convergent assembly of two comparably complex fragments, **14** and **19**, which were synthesized by coupling two simple cyclic ethers, **5** + **6** and **7** + **8**, respectively. It should be possible to improve the latest deprotection step. The present versatile synthetic strategy should be applicable for synthesizing the congeners (*8*) and should help accelerate the preparation of anti-ciguatoxin antibodies for detecting intoxicated ciguateric fish and create VSSC probes that may provide valuable insight into the VSSC-ligand interaction at the molecular level, as well as the activation and gating mechanism of VSSCs.

References and Notes

1. P. J. Scheuer, *Tetrahedron* **50**, 3 (1994).
2. R. J. Lewis, *Toxicon* **39**, 97 (2001).
3. R. Bagnis *et al.*, *Toxicon* **18**, 199 (1980).
4. M. Murata, A. M. Legrand, Y. Ishibashi, T. Yasumoto, *J. Am. Chem. Soc.* **111**, 8929 (1989).
5. M. Murata, A.-M. Legrand, Y. Ishibashi, M. Fukui, T. Yasumoto, *J. Am. Chem. Soc.* **112**, 4380 (1990).
6. M. Satake *et al.*, *J. Am. Chem. Soc.* **119**, 11325 (1997).
7. M. Satake, M. Murata, T. Yasumoto, *Tetrahedron Lett.* **34**, 1975 (1993).
8. T. Yasumoto *et al.*, *J. Am. Chem. Soc.* **122**, 4988 (2000).
9. Y. Shimizu, H.-N. Chou, H. Bando, *J. Am. Chem. Soc.* **108**, 514 (1986).
10. Y.-Y. Lin *et al.*, *J. Am. Chem. Soc.* **103**, 6773 (1981).
11. M.-Y. Dechraoui, J. Naar, S. Pauillac, A.-M. Legrand, *Toxicon* **37**, 125 (1999).
12. T. Yasumoto, M. Murata, *Chem. Rev.* **93**, 1897 (1993).
13. H. Oguri *et al.*, *Synthesis* 1431 (1999).
14. Y. Hokama *et al.*, *J. AOAC Int.* **81**, 727 (1998).
15. S. Pauillac *et al.*, *Toxicon* **38**, 669 (2000).
16. T. Anger, D. J. Madge, M. Mulla, D. Riddall, *J. Med. Chem.* **44**, 115 (2001).
17. W. A. Catterall, *Neuron* **26**, 13 (2000).
18. A. Lombet, J.-N. Bidard, M. Lazdunski, *FEBS Lett.* **219**, 355 (1987).
19. R. E. Gawley *et al.*, *Chem. Biol.* **2**, 533 (1995).
20. K. C. Nicolaou *et al.*, *Nature* **392**, 264 (1998).
21. K. C. Nicolaou *et al.*, *Chem. Eur. J.* **5**, 646 (1999).
22. K. C. Nicolaou *et al.*, *J. Am. Chem. Soc.* **117**, 10252 (1995).
23. H. Takakura, K. Noguchi, M. Sasaki, K. Tachibana, *Angew. Chem. Int. Ed.* **40**, 1090 (2001).
24. K. Kira, M. Isobe, *Tetrahedron Lett.* **42**, 2821 (2001).
25. K. Fujiwara, D. Takaoka, K. Kusumi, K. Kawai, A. Murai, *Synlett*, 691 (2001).
26. R. H. Grubbs, S. Chang, *Tetrahedron* **54**, 4413 (1998).
27. T. Oishi, Y. Nagumo, M. Hirama, *Chem. Commun.* (1998), p. 1041.
28. M. Maruyama, K. Maeda, T. Oishi, H. Oguri, M. Hirama, *Heterocycles* **54**, 93 (2001).
29. Md. A. Rahim, T. Fujiwara, T. Takeda, *Tetrahedron* **56**, 763 (2000).
30. T. Oishi *et al.*, *Chem. Commun.* (2001), p. 381.
31. H. Imai *et al.*, *Tetrahedron Lett.* **42**, 6219 (2001).
32. S. F. Sabes, R. A. Urbanek, C. J. Forsyth, *J. Am. Chem. Soc.* **120**, 2534 (1988).
33. S.-i. Fukuzawa, T. Tsuchimoto, T. Hotaka, T. Hiyama, *Synlett*, 1077 (1995).
34. K. Ishihara, Y. Karumi, M. Kubota, H. Yamamoto, *Synlett*, 839 (1996).
35. M. Inoue, M. Sasaki, K. Tachibana, *J. Org. Chem.* **64**, 9416 (1999).
36. S. Kim, J. Y. Do, S. H. Kim, D.-i. Kim, *J. Chem. Soc. Perkin Trans. 1* **17**, 2357 (1994).
37. E. Lee, J. S. Tae, C. Lee, C. M. Park, *Tetrahedron Lett.* **34**, 4831 (1993).
38. M. Sasaki, T. Noguchi, K. Tachibana, *Tetrahedron Lett.* **40**, 1337 (1999).
39. M. Sasaki, M. Inoue, T. Noguchi, A. Takeichi, K. Tachibana, *Tetrahedron Lett.* **39**, 2783 (1998).
40. G. C. Fu, S. T. Nguyen, R. H. Grubbs, *J. Am. Chem. Soc.* **115**, 9856 (1993).
41. M. Inoue, M. Sasaki, K. Tachibana, *Tetrahedron* **55**, 10949 (1999).
42. Y. Nagumo *et al. Bioorg. Med. Chem. Lett.* **11**, 2037 (2001).
43. Selected physical data, ^{1}H-NMR spectra, and CD spectra are provided as supplemental information on *Science* Online at www.sciencemag.org/cgi/content/full/294/5548/1904/DC1.

44. We thank T. Yasumoto for encouragement of this research and valuable information.

27 August 2001; accepted 29 October 2001

Engineering Crystal Symmetry and Polar Order in Molecular Host Frameworks

K. Travis Holman, Adam M. Pivovar, Michael D. Ward*

A crystal design strategy is described that produces a series of solid-state molecular host frameworks with prescribed lattice metrics and polar crystallographic symmetries. This represents a significant advance in crystal engineering, which is typically limited to manipulation of only gross structural features. The host frameworks, constructed by connecting flexible hydrogen-bonded sheets with banana-shaped pillars, sustain one-dimensional channels that are occupied by guest molecules during crystallization. The polar host frameworks enforce the alignment of these guests into polar arrays, with properly chosen guests affording inclusion compounds that exhibit second harmonic generation because of this alignment. This protocol exemplifies a principal goal of modern organic solid-state chemistry: the precise control of crystal symmetry and structure for the attainment of a specific bulk property.

The prediction of crystal structure based solely on the structure of molecular components remains one of the foremost challenges in organic solid-state chemistry (*1*–*3*). The inherent limitations of computational methods for structure prediction have forced solid-state chemists to rely on empirical crystal engineering strategies, which historically have been restricted to the design of general lattice architecture. In order to better manipulate the properties of organic solid-state materials and capitalize on their inherent versatility, however, crystal engineering needs to develop empirical models that provide reliable prediction and control of crystal symmetry, lattice parameters, and atomic positions.

In this regard, the synthesis of polar crystals from achiral molecular components has been a particularly noteworthy challenge, because it requires crystallization into acentric space groups (those lacking inversion symmetry) (*4*). Moreover, acentric space group symmetry is a requirement for a number of technologically relevant properties, including piezoelectricity, pyroelectricity, ferroelectricity, and second harmonic generation (SHG). SHG describes the ability of a material to double the frequency of incident light, a feature that is important to many advanced optoelectronics applications (*5*). Consequently, several approaches toward the achievement of acentric crystal packing have appeared in recent years; for example, acentric hydrogen-bonded aggregates (*6*, *7*), acentric metal-ligand coordination networks (*8*), antiparallel alignment of ionic sheets (*9*, *10*), and head-to-tail alignment of dipolar guests confined in channels of organic host lattices (*11*, *12*). Most strategies, however, have not emphasized precise control of the three-dimensional (3D) crystal structure, focusing instead on the frustration of centric packing, so that the tendency to form acentric crystals is increased. We describe here a crystal design strategy that produces polar host frameworks with 3D crystal symmetries and lattice metrics that are preordained by the structure and symmetry of the molecular components. These new polar host frameworks guide the alignment of selected guest molecules into

Department of Chemical Engineering and Materials Science, University of Minnesota, 421 Washington Avenue Southeast, Minneapolis, MN 55455, USA.

*To whom correspondence should be addressed. E-mail: wardx004@umn.edu

polar arrays, affording inclusion compounds that exhibit SHG activity.

Our laboratory has reported a series of lamellar host frameworks constructed from guanidinium and organodisulfonate ions, in which the organic residues of the organodisulfonate ions serve as molecular pillars that support inclusion cavities between opposing hydrogen-bonded sheets of complementary guanidinium (G) ions and sulfonate (S) moieties (Fig. 1) (*13–16*). The GS sheet can be described as being made up of 1D GS "ribbons" that are fused along their edges by hydrogen bonds that serve as hinges. These hinges allow accordionlike puckering of the sheet, about an angle θ_{IR}, effectively allowing the host to shrink-wrap around the guest molecules so that crystal packing is optimized (*17*). The organodisulfonate pillars can project up or down from any S site on the GS sheet, enabling the formation of numerous framework architectures (*18*). The most common architectures are the "bilayer" (not shown in Fig. 1) and the "simple brick," the latter being continuous in all three dimensions as a consequence of alternating up-down pillar orientations on adjacent GS ribbons. The lattice parameter *a*, which is equivalent to the S···S distance along the GS ribbon, is essentially constant for different GS compounds. In the simple brick framework, in which puckering can be substantial, the lattice parameters *b* and *c* depend on θ_{IR}, according to simple mathematical functions (Fig. 1B). The *c* lattice parameter also depends on the length of the organodisulfonate pillar, denoted as *l*. The three lattice directions are mutually orthogonal in an ideal simple brick framework, resulting in an orthorhombic lattice. Slight deviations from the ideal orthorhombic symmetry, however, are common, owing to the softness of the host framework.

Almost all of the simple brick GS compounds examined previously have been constructed with linear achiral pillars, in which the sulfonate substituents are located at opposite ends, with the C–S bond vectors antiparallel [for example, 1,4-benzenedisulfonate (Scheme 1)]. Although we have observed isolated examples of polar ordering of certain guest molecules in these compounds, simple brick frameworks with linear pillars, whether puckered or unpuckered, are not inherently acentric and typically form centric inclusion compounds (*19*).

A simple model can be used to devise a protocol, based entirely on achiral components, for achieving an acentric polar version of the simple brick framework (Fig. 2). Beginning with a puckered GS host with linear pillars, it is apparent that puckering of the GS sheet forces the pillars in adjacent layers to tilt in opposite directions. An imaginary dissection of these pillars reveals that the brick framework actually consists of an equal number of sheets with dipoles aligned in opposite directions, hence affording a centric framework. A 180° rotation of every other sheet in the lamellar stack, about an axis orthogonal to the sheets (that is, *c*), would produce an ensemble of sheets with all of their dipoles parallel. Reconnection of the pillars, now banana-shaped because the C–S bond vectors adopt a bent configuration rather than a linear one, would produce a host framework in which all the pillars point in the same direction, in this case establishing a polar axis along *b* (*20*). The geometry of the banana-shaped pillars, which remain connected to the GS sheets,

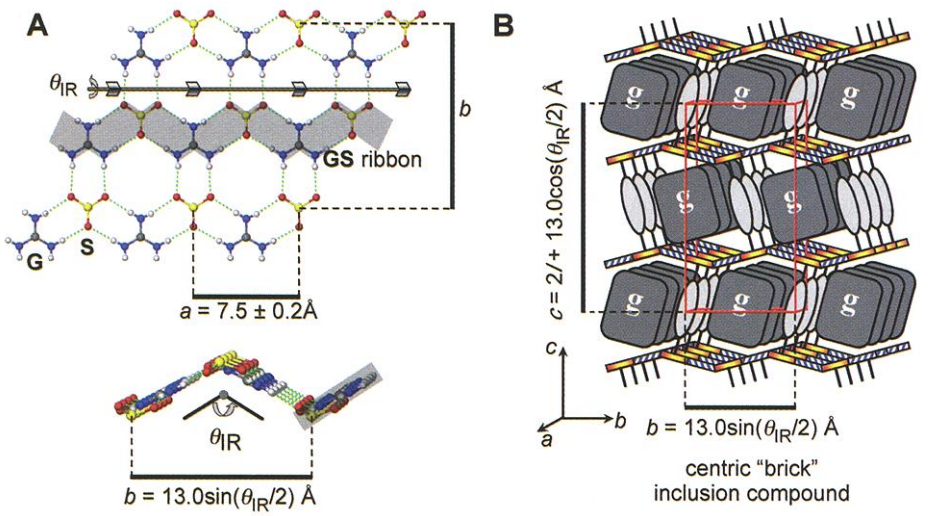

Fig. 1. (**A**) Top and side views of the GS sheet (black, carbon; blue, nitrogen; white, hydrogen; yellow, sulfur; red, oxygen). The sheet consists of (G)N–H···O(S) hydrogen-bonded ribbons (highlighted in gray) fused laterally by (G)N–H···O(S) hydrogen bonds. (**B**) Schematic representation of a simple brick inclusion compound with puckered GS sheets. The G ions are blue, the organodisulfonate pillars are shaded light gray, and the S moieties are yellow and red. The ideal orthorhombic unit cell, defined by the lattice constants *a*, *b*, and *c*, is outlined in red. The included guest molecules are schematically depicted as gray squares inscribed with the letter g.

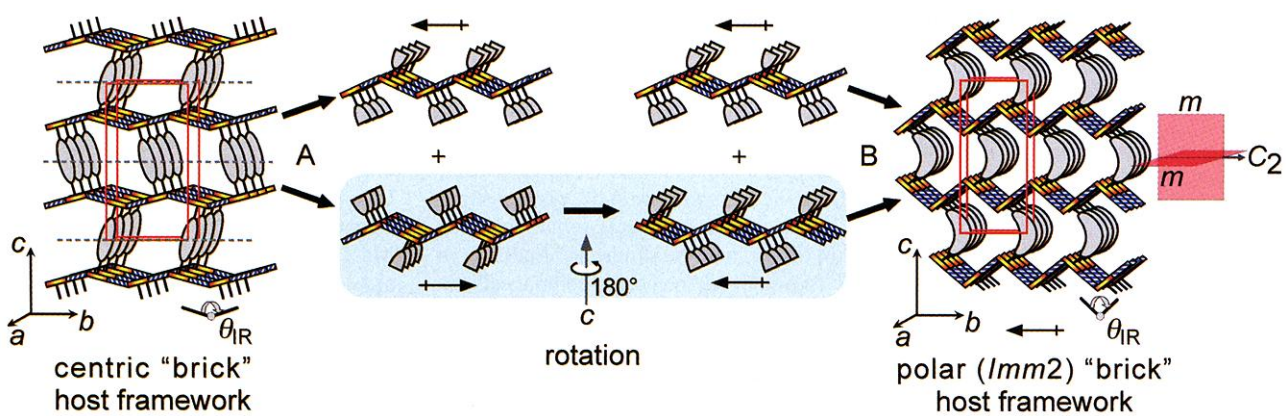

Fig. 2. Schematic representation of the strategy for designing 3D polar host frameworks (and, consequently, polar crystals): A simple brick GS host framework derived from linear achiral organodisulfonate pillars, such as 1,4-benzenedisulfonate (BDS). Dissection (**A**) of the pillars illustrates that the individual GS sheets have a polar axis and that the dipoles of adjacent sheets are antiparallel. Rotation of one-half of the GS sheets by 180° about the *c* axis, illustrated here for one sheet (highlighted in blue) of an adjacent pair, aligns all the GS sheet dipoles parallel. Reconnection (**B**) of the reoriented sheets affords a brick framework in which the now banana-shaped organodisulfonate pillars force the formation of a polar host framework. The dipole directions illustrated here are intended only as a guide to describe the orientation of the GS sheets.

would now force puckering of the sheets (rather than puckering being driven by the tendency to optimize packing of the pillars and guests). This in turn encourages the formation of the brick architecture instead of the bilayer form, which cannot achieve highly puckered configurations. If the two C–S bond vectors are precisely normal to the GS ribbons, the puckering angle will be dictated by the "bend angle"; that is, the angle defined by the intersection of the two C–S bond vectors. More important, it is apparent from this model that all simple brick host frameworks constructed with banana-shaped pillars will have polar symmetry.

This surmise can be extended even further to the prediction of space group symmetry. Inspection of Fig. 2B reveals that if the banana-shaped pillar possesses C_{2v} symmetry, with two mirror planes bisecting the pillar and intersecting on a twofold axis (Fig. 2), the space group symmetry of the resulting ideal host framework can be assigned as orthorhombic *Imm*2 (*21*). Such a framework, which would be polar but not chiral, would probably guide the polar ordering of guest molecules contained within its inclusion cavities.

The strategy embodied in Fig. 2 has been reduced to practice for single-crystal inclusion compounds based on GS hosts constructed with three different banana-shaped pillars: mesitylenedisulfonate (MDS), 2,4,5,6-tetramethylbenzene-1,3-disulfonate (TMBDS), and 2-methoxy-4,6-dimethyl-1,5-benzenedisulfonate (MDBDS), each having a bend angle of 120° (Scheme 1) (*22*). The first two pillars in this series possess the nominal C_{2v} molecular symmetry required for ideal *Imm*2 space group symmetry, whereas the third possesses C_s point group symmetry (*23*). Given the length of the pillars (5.5 Å, as measured by the intramolecular S···S distance) and the 120° bend angle, the anticipated lattice parameters for these frameworks, based on their orthorhombic symmetry and the equations provided in Fig. 1B, are a = 7.5 Å, b = 11.3 Å, c = 21.2 Å, and $\alpha = \beta = \gamma = 90°$. The ideal puckering angle, based on the bend angle, is $\theta_{IR} = 120°$.

The G_2MDS, G_2TMBDS, and G_2MDBDS hosts readily form crystalline inclusion compounds with a variety of simple guests such as mesitylene, nitrobenzene, and dioxane/methanol. Single-crystal structure determinations of these inclusion compounds (Table 1) revealed that these hosts adopt the anticipated polar architecture with highly puckered GS sheets and banana-shaped pillars, all pointing along the polar b axis of the crystals (Fig. 3A). The included guest molecules are confined within 1D corrugated channels, flanked by pillar "walls," along the b axis. The maximum possible orthorhombic space group symmetry anticipated by the protocol in Fig. 2, *Imm*2, is realized in crystals of G_2MDS·(mesitylene), G_2MDS·(nitrobenzene) (Fig. 3, B and C) and G_2TMBDS·(nitrobenzene). The achievement of *Imm*2 symmetry by these inclusion compounds is possible because these guests can have C_{2v} molecular symmetry (the nitrobenzene guests in the crystal actually exhibit disorder about the *ab* mirror plane with overall C_{2v} symmetry). The host framework in G_2MDBDS·(dioxane)·(methanol) exhibits an essentially identical polar architecture. The

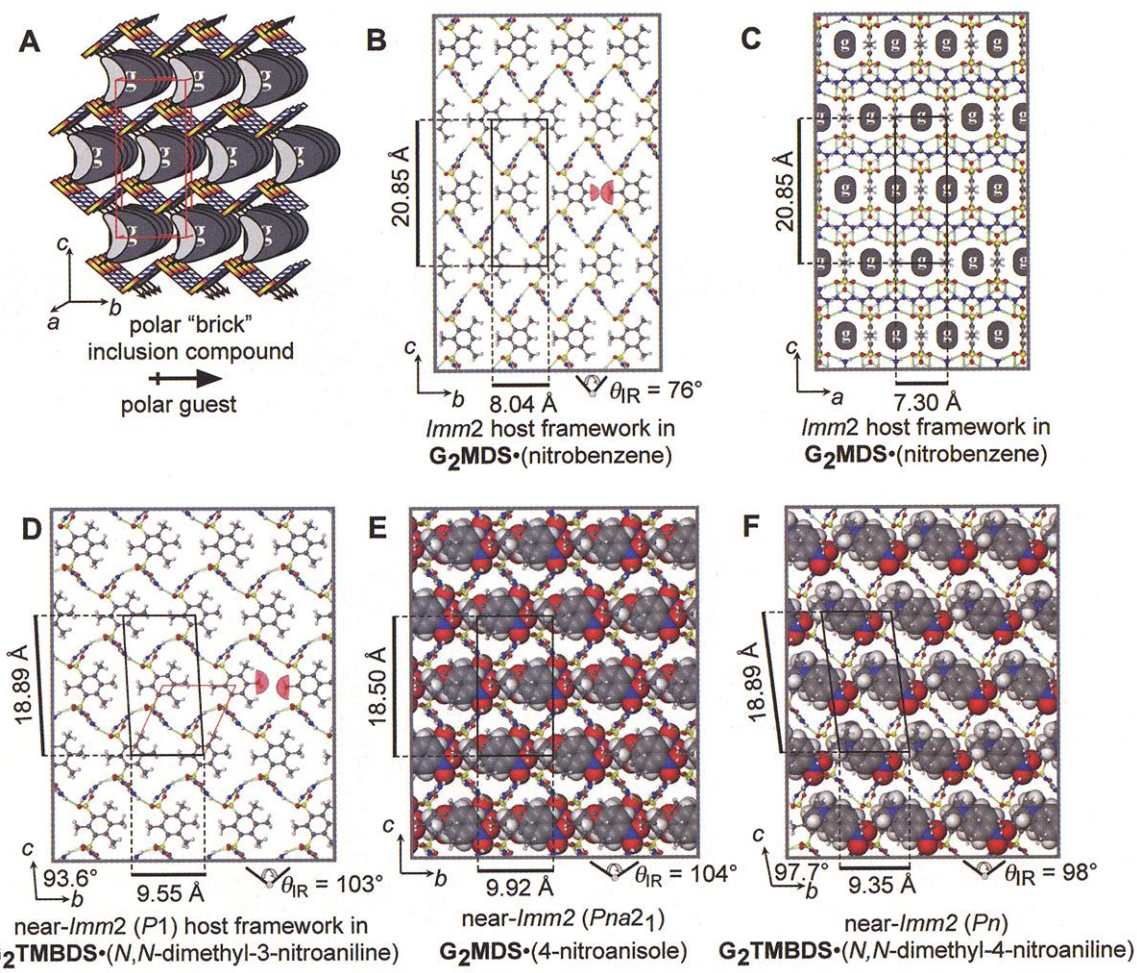

Fig. 3. (**A**) Schematic representation of polar simple brick GS host frameworks occupied by guest molecules (gray), which form polar arrays. (**B**) The orthorhombic *Imm*2 polar brick host framework (the polar guest arrays have been omitted for clarity) in G_2MDS·(nitrobenzene), as viewed perpendicular to the corrugated guest-filled channels. The red shading on the opposing ends of one pair of adjacent pillars corresponds to van der Waals radii of the substituents. (**C**) The framework in (B) as viewed parallel to the channels, with the guests depicted as gray ovals. (**D**) The near-*Imm*2 (actual *P*1 symmetry, unit cell depicted in red) host framework in G_2TMBDS·(*N*,*N*-dimethyl-3-nitroaniline). The polar guest arrays have been omitted for clarity. The large *N*,*N*-dimethyl-3-nitroaniline guest prevents close contact of adjacent pillars along the b axis, as indicated by the red van der Waals spheres. (**E**) The crystal structure of SHG-active G_2MDS·(4-nitroanisole). (**F**) The crystal structure of SHG-active G_2MDBDS·(*N*,*N*-dimethyl-4-nitroaniline). In (E) and (F), the guests are rendered in space-filling and the hosts in ball-and-stick format.

symmetry of the framework, however, is reduced (to *Pn*), in part by the lower C_s symmetry of the MDBDS pillar. As expected, the host framework in each compound guides the assembly of the guest molecules into a polar array, in which all the guests are oriented along *b*.

Based on the crystal structures with these simple guests, it was anticipated that the polar GS hosts would also enforce polar alignment of guest molecules with significant molecular second-order nonlinear optical hyperpolarizabilities (β), thereby producing materials with SHG activity (*24*, *25*). Notably, *mm*2 point group symmetry is recognized as effective for SHG (*26*). In this regard, G_2MDS and G_2TMBDS form 1:1 inclusion compounds with *N,N*-dimethyl-3-nitroaniline (β_{1064nm} = 25) and 4-nitroanisole (β_{1064nm} = 65). The inclusion of *N,N*-dimethyl-4-nitroaniline (β_{1064nm} = 218), however, could only be achieved in G_2TMBDS. Single-crystal structure analysis of these compounds confirmed the existence of the polar host architecture, with the guests organized as polar arrays along the *b* axis. Although these compounds do not exhibit strictly orthorhombic *Imm*2 symmetry, the lattice parameters for each compound reveal that their frameworks are nearly indistinguishable from the ideal *Imm*2 form (*27*). This can be illustrated by G_2TMBDS·(*N,N*-dimethyl-3-nitroaniline); though crystallizing in *P*1, the lowest space group symmetry possible, its framework displays an architecture nearly identical to ideal *Imm*2 (Fig. 3D).

None of these inclusion compounds exhibit head-to-tail disorder of the dipolar guests, which is sometimes observed in other channel-type inclusion compounds. A head-to-tail configuration of the guests favors polar ordering within each channel of the GS hosts; however, the large interchannel distances would preclude significant guest-guest dipole interactions between channels. Although the anisotropic structure of the channels in the polar GS hosts may play a shape-directing role in establishing polar guest order, the dipole orientations of the various guest molecules, relative to the banana-shaped pillars, are essentially identical in all the inclusion compounds, despite the different sizes and shapes of the guests. This suggests that the uniform polar alignment of the guest molecules, both within each channel and between channels, can be ascribed largely to the inherently dipolar character of the host framework, which creates an environment in which host-guest interactions anchor the guests into the 3D polar arrays.

It is apparent that the banana-shaped pillars force puckering of the GS sheet to produce the expected polar architecture. In every case, however, θ_{IR} is lower than the ideal value of 120°. This feature, as well as the slight tilting of the C–S bond vectors from normality with the GS ribbons, reflects the tendency of the molecular components to strive for close packing along the *b* axis. The lower compression limits of *b* are in fact determined by steric repulsion along this direction, either between the pillars or between the guests. Considering only the steric limits imposed by pillars (Scheme 1), the lower limits of *b* for G_2MDS and G_2TMBDS are 8.0 and 8.9 Å, respectively, which correspond to minimum puckering angles of θ_{IR} = 76° and 86°. The corresponding *c* values also fall within the ranges expected for each pillar. Although estimations of the anticipated lower limits of *b* and θ_{IR} for G_2MDBDS are somewhat complicated by the conformational freedom of the methoxy group, models suggest that the lower limit for *b* is slightly greater than 8.0 Å.

All the inclusion compounds in Table 1 exhibit *b* values between the ideal value of 11.3 Å and their respective lower limits. The relatively small guests in G_2MDS·(nitrobenzene) and G_2TMBDS·(nitrobenzene) result in *b* values of 8.04 and 9.22 Å, respectively, which are near the pillar-limited values for these hosts (as illustrated by the red van der Waals hemispheres for G_2MDS in Fig. 3B). Conversely, the *b* values for G_2MDS·(*N,N*-dimethyl-3-nitroaniline) and G_2TMBDS·(*N,N*-dimethyl-3-nitroaniline) are nearly identical (9.56 and 9.55 Å, respectively), reflecting steric compression governed by this larger guest rather than the pillars. In these cases, the pillars are not closely

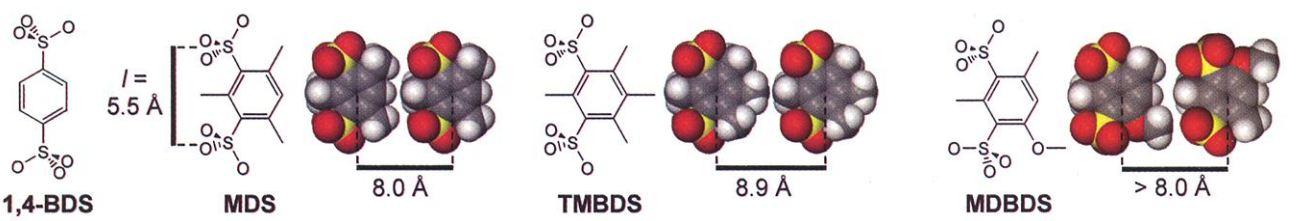

Scheme 1.

Table 1. Structural parameters and SHG activity for *Imm*2 and near-*Imm*2 polar brick inclusion compounds.

Compound	Space group	a (Å)	b (Å)	c (Å)	α (°)	β (°)	γ (°)	*V* (Å³)	θ_{IR} (°)	SHG‡
Anticipated framework (C_{2v} pillars)*	*Imm*2	7.5	11.3	17.5	90	90	90	1483	120	
Fully compressed G_2MDS framework†	*Imm*2†	7.5	8.0	21.2	90	90	90	1272	76	
Fully compressed G_2TMBDS framework†	*Imm*2†	7.5	8.9	20.5	90	90	90	1368	86	
G_2MDS · (mesitylene)	*Imm*2	7.39	8.24	20.71	90	90	90	1261	80	<1
G_2MDS · (nitrobenzene)	*Imm*2	7.30	8.04	20.85	90	90	90	1224	78	<1
G_2MDS · (*N,N*-dimethyl-3-nitroaniline)	*P*1	7.62	9.56	18.55	85.9	80.8	89.3	1330	103	1
G_2MDS · (4-nitroanisole)	$Pna2_1$	7.39	9.92	18.50	90	90	90	1357	104	4
G_2TMBDS · (mesitylene)	*C*2	7.56	9.21	19.16	90	94.6	90	1329	97	<1
G_2TMBDS · (nitrobenzene)	*Imm*2	7.43	9.22	19.30	90	90	90	1321	96	<1
G_2TMBDS · (*N,N*-dimethyl-3-nitroaniline)	*P*1	7.63	9.55	18.46	86.4	82.7	89.6	1332	103	1
G_2TMBDS · (4-nitroanisole)	*Cm*	7.40	9.52	18.45	95.2	90	90	1293	102	4
G_2TMBDS · (*N,N*-dimethyl-4-nitroaniline)	*Pn*	7.45	9.35	18.89	97.7	90	90	1304	98	10
G_2MDBDS · (dioxane) · (methanol)†	*Pn*	7.88	8.63	19.63	90	90	94.4	1331	88	<1

*The lattice parameters *a*, *b*, and *c* used here represent orthogonal vectors that are strictly appropriate only for host frameworks with orthorhombic symmetry. The lattice parameters of the near-orthorhombic frameworks have been transformed to this convention for convenient comparison. The anticipated values of *b*, *c*, θ_{IR}, and *V* are predicated on pillars with a 120° bend angle and a length (*l*) of 5.5 Å (Fig. 1 and Scheme 1). †The fully compressed values are predicated on the close-packing limit between the pillars along *b*. The fully compressed limit for G_2MDBDS is more difficult to establish because of the conformational freedom of the methoxy group. The expectation of *Imm*2 symmetry is based on on assumed C_{2v} pillar symmetry [see (*23*)]. ‡SHG response relative to values for KDP as measured by the Kurtz-Perry powder method.

packed along the *b* axis. Attempts to synthesize polar simple brick frameworks with related banana-shaped 1,3-benzene- and 2,4-dimethyl-1,5-benzenedisulfonates have failed. This most likely reflects excessive void space created by the absence of methyl substituents in key positions, including those projecting along the *b* axis (*28*).

A preliminary measurement of the SHG activity of these materials, using the Kurtz-Perry powder method (*29*), reveals that, as one would expect, the response scales according to the β values of the included guests. The highest SHG activity measured, in G_2TMBDS·(*N,N*-dimethyl-4-nitroaniline), is 10 times that measured for potassium dihydrogen phosphate (KDP), an accepted SHG standard. G_2MDS·(mesitylene) and G_2TMBDS·(mesitylene), which contain a centric guest with no nonlinear optical activity, do not exhibit any measurable SHG response. Therefore, the polar host framework does not contribute significantly to the SHG activity, and the SHG activity is primarily associated with the polar guest arrays. This illustrates the fact that inclusion compounds can permit crystal architecture, provided by the host framework, to be separated from function introduced by the included guests, in this case SHG. The ionic GS host frameworks also bestow thermal stability (the inclusion compounds are stable to at least 180°C) on otherwise low-melting guests, an important consideration for nonlinear optics applications.

These results demonstrate that crystal engineering, using a protocol based on simple geometric principles, can include the prediction and control of lattice metrics and nominal space group symemtry. The ability to predict crystal structure with this level of detail is a rather unusual achievement in organic solid-state chemistry (*30*). Furthermore, this design produces a polar host framework from entirely achiral components, resulting in polar alignment of guest molecules that do not crystallize in polar space groups in their pure forms or that exist as liquids at room temperature. We anticipate that related frameworks constructed with pillars having significant hyperpolarizabilities also can produce materials with SHG activity.

References and Notes

1. P. Ball, *Nature* **281**, 648 (1996).
2. A. Gavezzotti, *Acc. Chem. Res.* **27**, 309 (1994).
3. J. Maddox, *Nature* **201**, 335 (1988).
4. D. Y. Curtin, I. C. Paul, *Chem. Rev.* **81**, 525 (1981).
5. C. Bossard, *et al.*, in *Crystal Engineering: From Molecules and Crystals to Materials*, D. Braga, F. Grepioni, Eds. (Kluwer, Dordrecht, Netherlands, 1991), pp. 251–268.
6. M. C. Etter, K. S. Huang, *Chem. Mater.* **4**, 824 (1992).
7. M. S. Wong, V. Gramlich, C. Bosshard, P. Günter, *J. Mater. Chem.* **7**, 2021 (1997).
8. W. Lin, O. R. Evans, R.-G. Xiong, Z. Wang, *J. Am. Chem. Soc.* **120**, 13272 (1998).
9. S. R. Marder, J. W. Perry, W. P. Schaefer, *Science* **245**, 626 (1989).
10. S. R. Marder, J. W. Perry, W. P. Schaefer, C. P. Yakymyshyn, *Chem. Mater.* **6**, 1137 (1994).
11. W. Tam *et al.*, *Chem. Mater.* **1**, 128 (1989).
12. O. Konig, H.-B. Burgi, Th. Armbruster, J. Hulliger, Th. Weber, *J. Am. Chem. Soc.* **119**, 10632 (1997).
13. V. A. Russell, C. C. Evans, W. Li, M. D. Ward, *Science* **276**, 575 (1997).
14. K. T. Holman, M. D. Ward, *Angew. Chem. Int. Ed.* **39**, 1653 (2000).
15. J. A. Swift, A. M. Pivovar, A. M. Reynolds, M. D Ward, *J. Am. Chem. Soc.* **120**, 5887 (1998).
16. V. A. Russell, M. C. Etter, M. D. Ward, *J. Am. Chem. Soc.* **116**, 1941 (1994).
17. K. T. Holman, A. M. Pivovar, J. A. Swift, M. D. Ward, *Acc. Chem. Res.* **34**, 107 (2001).
18. K. T. Holman, S. M. Martin, D. P. Parker, M. D. Ward, *J. Am. Chem. Soc.* **123**, 4421 (2001).
19. J. A. Swift, M. D. Ward, *Chem. Mater.* **12**, 1501 (2000).
20. The term banana-shaped has also been used to describe thermotropic liquid crystal compounds [G. Pelzl, S. Diele, W. Weissflog, *Adv. Mater.* **11**, 707 (1999)].
21. According to the defined axes *a*, *b*, and *c* in Fig. 2, the space group assignment must strictly be *Im2m*. For clarity, however, the discussion adopts the standard crystallographic notation of *Imm2* for this space group, with the understanding that the notations are related by a simple transformation of the *b* and *c* axes. The *I*-centering condition is enforced by the connectivity of the pillars and sheets, with adjacent sheets being offset along the *a* axis by exactly *a*/2.
22. The strategy used here based on GS inclusion compounds constructed from banana-shaped pillars is not related to the factors that govern polar ordering in crystals of meta-disubstituted benzenes, which crystallize more often in polar space groups than do their para- or ortho-substituted derivatives because of simple packing considerations [L. S. Rez, *Kristallographie* **5**, 63 (1960) and A. C. Skrapski, *J. Chem. Soc. Perkin Trans.* **2**, 1197 (1973)].
23. Strictly speaking, the MDS and TMBDS pillars do not possess perfect C_{2v} symmetry, owing to the reduction of symmetry by the methyl hydrogens (in the absence of free rotation of the methyl group) and steric forces that cause minute out-of-plane distortions of the substituents [A. Koeberg-Telder, H. Cerfontain, C. H. Stam, G. Kreuning, *Recl. Trav. Chim. Pays-Bas* **106**, 142 (1987); M. A. M. Meester, H. Schenk, *Recl. Trav. Chim. Pas-Bas* **91**, 213 (1972)].
24. D. S. Chemla, J. Zyss, *Nonlinear Optical Properties of Organic Molecules and Crystals*, vol. 1 and 2 (Academic Press, Orlando, FL, 1987).
25. *Nonlinear Optical Effects and Materials*, P. Gunter, Ed. (Springer Series in Optical Sciences, vol. 72, Berlin, Germany, 2000).
26. J. Zyss, J. L. Oudar, *Phys. Rev. A* **26**, 2028 (1982).
27. The lattice parameters *a*, *b*, and *c* depicted in Fig. 2 represent orthogonal vectors that are strictly appropriate only for host frameworks with orthorhombic symmetry. The near-*Imm2* frameworks are a consequence of slight deviations of the *a*, *b*, and/or *c* axes from orthogonality, with concomitant losses of one or more mirror planes, C_2, and/or screw axes because of the fixed guest orientations. The real lattice parameters of these lower symmetry frameworks have been transformed to the orthorhombic convention for convenient comparison in Table 1.
28. Though we have not observed any inclusion compounds with 1,3-benzene- and 2,4-dimethyl-1,5-benzenedisulfonates, other GS host framework architectures are possible with banana-shaped pillars. For example, double-brick architectures have been observed in G_2MDS and G_2MDBDS with guests other than those described here (*18*).
29. S. K. Kurtz, T. T. Perry, *J. Appl. Phys.* **39**, 3798 (1968).
30. M. E. Brown, J. D. Chaney, B. D. Santarsiero, M. D. Hollingsworth, *Chem. Mater.* **8**, 1588 (1996).

31. Supported in part by the Materials Research Science and Engineering Center program of NSF under award number DMR-9809364 and the NSF Division of Materials Research (DMR-9908627). K.T.H. gratefully acknowledges a postdoctoral fellowship from Natural Sciences and Engineering Research Council of Canada. We also thank V. Young Jr. for crystallographic assistance.

16 July 2001; accepted 1 November 2001

Seismic Detection of Rigid Zones at the Top of the Core

Sebastian Rost* and Justin Revenaugh

Data from earthquakes in the Tonga-Fiji region recorded at a seismic array in northern Australia show evidence for rigid zones at the top of the outer core. The *ScP* waveforms can be modeled by thin (0.12 to 0.18 kilometer) zones of molten iron mixed with solid material with a small, but positive, *S*-wave velocity (0.6 to 0.8 kilometer per second) that enables the propagation of *S*-waves in the outermost core. The zones may be topographic highs of the core-mantle boundary filled by light core sediments and might be important for variation of Earth's nutation and for convection of the outer core.

The core-mantle boundary (CMB) region, where the molten iron outer core meets the solid silicate mantle, represents the largest compositional and rheological contrast in Earth's interior. Strong lateral variations of *S*- and *P*-wave velocity exist in the lowermost 200 to 300 kilometers of the mantle above the CMB (*1–4*), a region capped in many places by a sharp discontinuity (*5, 6*). In the lowermost few tens of kilometers of the mantle, ultralow-velocity zones (ULVZ) have been detected (*7–9*) and interpreted as evidence for partial melt or chemical contamination of the lowermost mantle by the outer core (*10–12*). Both explanations have significant implications for core and mantle dynamics (*13–16*). ULVZ are discussed as source regions of mantle plumes and may control the frequency of Earth's magnetic field reversals (*17, 18*). Recently, models of the CMB with

Department of Earth Sciences, University of California, Santa Cruz, CA 95064, USA.

*To whom correspondence should be addressed. E-mail: srost@es.ucsc.edu